International Journal of GEOMATE, Aug., 2022, Vol.23, Issue 96, pp.104-111
ISSN: 2186-2982 (P), 2186-2990 (O), Japan, DOI: https://doi.org/10.21660/2022.96.3328
Geotechnique, Construction Materials and Environment

COMPARATIVE STUDY OF THE BEHAVIORS OF SKIRTED FOUNDATIONS OF DIFFERENT SHAPES

*Kyrillos Magdy[1], Ayman Altahrany[2] and Mahmoud Elmeligy[3]

[1, 2, 3] Faculty of Engineering, Mansoura University, Egypt

*Corresponding Author, Received: 23 Feb. 2022, Revised: 20 May 2022, Accepted: 12 June 2022

ABSTRACT: Structural skirts are vertical or inclined walls that encircle the soil mass beneath the footing. They improve shallow footing load-settlement behavior by restricting the soil and containing the soil plastic flow. Limited studies comparing the load-settlement behaviors of skirted foundations of different shapes are available. Therefore, this study highlights the effects of skirts on the load-settlement behavior of shallow footing through a comparative study of the behavior of square and circular footing. Fourteen small-scale physical models were developed on a circular and square footing with different skirt depths to investigate the effect of skirt depth, skirt cell shape, and footing shape. 3D finite element models were conducted through experimental findings using PLAXIS 3D software. Results show that using the aforementioned skirted foundations improves the load-settlement behavior of loose sandy soil more effectively than compacted soil, making them a good alternative to deep foundations for soft soil at the surface. Under the current study conditions and variables, such skirts increase the ultimate load by up to 5.67 and 8.97 times for square and circular footing having a skirt depth ratio of 1.50, respectively. Furthermore, the reduction in settlement for the shallow footing is found to be >61.8%. This study illuminated the effect of skirt cell shape, where the improvement in the load-settlement behavior was greater for the circular skirted footing than for the square when both had the same width and skirt depth. The finite element results of the load-settlement curves and bearing capacities were in close agreement with the experimental findings.

Keywords: Skirted foundation, Circular footing, Square footing, Experimental study, Numerical analysis

1. INTRODUCTION

Geotechnical engineers are constantly seeking new soil improvement techniques that could help obtain ideal soil behaviors. These techniques have a great influence on the overall soil behavior, such as increasing the bearing capacity of the soil and reducing its settlement. These improvement techniques include compaction, reinforcement, and grouting. However, most of these technologies are costly and are influenced by the groundwater level and site conditions. One improvement technique is the use of structured skirts; this technique has many advantages. For instance, it does not necessitate any soil excavation, and it is not affected by the groundwater level. Structure skirts are used widely in coastal and offshore structures where scouring is a major problem. Researchers [1,2,3] have investigated the effect of using skirts in such applications. However, only few studies have focused on the behaviors of skirted foundations resting on loose sand, which are used as conventional footings for residential and commercial structures Certain researchers [4,5,6,7] have evaluated the behaviors of skirted foundations; they investigated the behaviors of skirted foundations using an experimental small-scale model; such foundations were investigated using finite element analysis and a small-scale laboratory model [8,9]. These studies helped to evaluate the bearing capacity and soil settlement for this investigation.

The best way for studying foundation engineering problems is to conduct full-scale field tests that can compensate for the random soil properties. However, because of the limited budget and the lack of case studies, a laboratory experimental small-scale model was used for this research. Although this small model had certain limitations, such as boundary conditions and scale effect, it produced comparatively satisfactory results. Therefore, this study investigates the skirted footing behavior by investigating different shapes of skirted footing using small-scale physical models. These footings are rested over soft soil like loose sand and subjected to vertical load, which can be used as conventional footings for residential and commercial structures.

2. RESEARCH SIGNIFICANCE

This paper focuses on the skirted footing response under compression loads where the footing is supported by loose sand. A comparison of square and circular small-scale footings highlighted the influence of the skirt cell shape and footing shape effect. Furthermore, the effect of the skirt depth (D_s) on the bearing capacity was investigated. The effectiveness of using this type of footing as a settlement reducer was explored.

Finally, to help other researchers fabricate full-scale 3D models, a 3D finite element model was validated using the experimental results of this research.

3. TESTING EQUIPMENT

To achieve rigid conditions, a surface footing model was fabricated using a rigid steel plate of 20-mm thickness. The footings used were of two shapes: circular and square. The diameter (D) of the circular footing and the width (B) of the square footing were both chosen as 60 mm (see Fig. 1).

The vertical skirts consisted of rigid steel plates having 2.5-mm thickness for the circular skirts and 2.00-mm thickness for the square skirts. The skirts had side holes at intervals equal to 0.25B or 0.25D. These holes had two advantages. The first advantage was that they let the trapped air escape while installing the skirt into the soil; the second advantage was that they let the footing move up and down at intervals of 0.25B or 0.25D to achieve the required skirt depth. The skirts were attached firmly and accurately to the footing using two bolts. The skirt depth was measured after it was bolted with the footing. The depth ratios (Ds/D or Ds/B) of the skirts were 0.25, 0.50, 0.75, 1.00, 1.25, and 1.50 (Fig.1).

The test tank was made of rigid steel of 3-mm thickness with inside circular stiffeners to avoid any deformation. The inside diameter of the cylindrical tank was 354 mm, and its height was 550 mm. The sand within the tank was at a height of 400 mm. The maximum footing dimension was 60 mm, and the maximum skirt depth was 90 mm. The tank's breadth was 5.9 times the width of the footing. The depth beneath the highest skirt was 5.17 times the width of the footing. Also, while testing, it was noted that using these dimensions did not have any effect on the failure mechanism, and no bulging was noticed around the footing. Therefore, these dimensions were adequate to eliminate any rigid boundary effect.

The loading frame consisted of a motor inside to achieve a strain rate condition ranging from 0.1 to 5 mm/min. It had a key to control the raising and lowering of the movable cap, which fulfilled the strain condition. The attached steel frame had a maximum clear span of 364 mm and a height of 1150 mm; these dimensions were adequate for the test tank. The proving ring was first attached to the upper fixed frame. Then, the shaft was connected to the proving ring. The linear variable differential transformer (LVDT) was attached to the top fixed frame with this system by a magnetic base. The load was centered using a small cap of 40-mm diameter to allow the footing to settle only in the vertical direction. The use of one dial gauge was acceptable because of two reasons. The first reason was that the footing was allowed to settle in one direction. The second reason was that the footing had small dimensions. The same setup was used by [10]. The following diagram shows the overall arrangement of the equipment used in this investigation (Fig. 2).

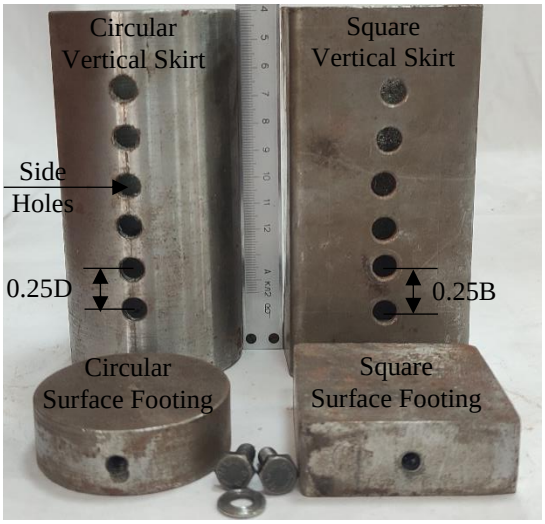

Fig.1 Surface footing and the vertical skirts used

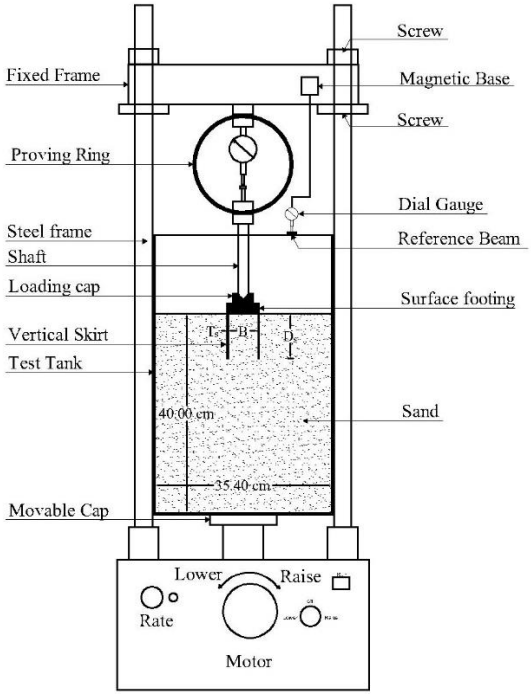

Fig. 2 Complete setup of the testing apparatus

4. EXPERIMENTAL PROCEDURE

4.1 Test Material

The sand was brought from Gamasa City and dried in an oven for one day. Then, it was sieved in sieves having diameters of 4.75 mm and 0.075 mm.

The sand used in this research had been passed through a 4.75-mm sieve but was retained in a 0.075-mm sieve. Fig. 3 shows the grain size distribution. The properties of the sand used in the experiment were obtained through laboratory tests, and they are listed in Table 1.

Table 1 Sand properties used in the tests

Property	Value
Specific gravity, G_s	2.68
Effective particle size, D_{10} (mm)	0.164
Average particle size, D_{50} (mm)	0.29
Uniformity coefficient, C_u	1.98
Coefficient of curvature, C_c	0.87
Maximum dry unit weight, $\gamma_{d\max}$ (t/m^3)	1.728
Minimum dry unit weight, $\gamma_{d\min}$ (t/m^3)	1.482
Average relative density, D_r (%)	35
The angle of internal friction, ϕ (°)	34.5
Maximum void ratio, e_{max}	0.81
Minimum void ratio, e_{min}	0.55

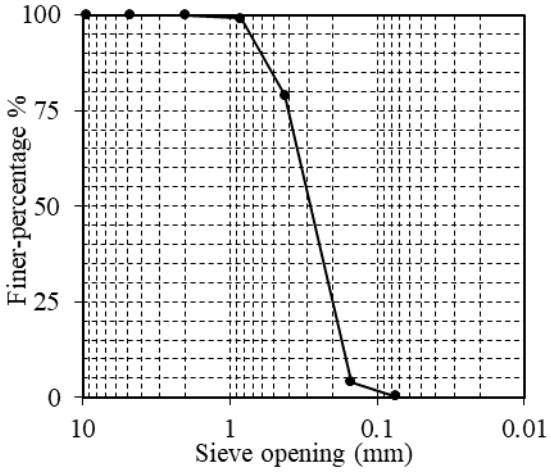

Fig. 3 Curve showing the distribution of sand particle sizes

4.2 Test Tank Preparation

For homogeneity of the sand sample, it was layered five times in the test tank, each layer was 80-mm thick, which gave a total height of 400 mm of sand inside the test tank. A vertical load test was performed at a relative density of 35%. The volume of each layer was calculated. The weight of each layer was measured using a balance having an accuracy of 0.01 gm, and the layer was compacted with a 585.28-gm rammer to achieve the desired relative density by trial and error. The testing schedule shown in Table 2 was followed. After each layer was placed, it was compacted to the desired relative density. Then, the top surface was sharpened before adding the next layer of soil. Then, this step was repeated to level up the sand to 400 mm. The footing was then placed on the surface of the compacted sand. The footing was positioned horizontally on the top surface before being driven vertically in the sand at a constant rate. To avoid over-or under-installation of the footings, the operation was carefully performed through the side holes of the skirt; the top surface of the sand was visible. Furthermore, the driving depth and the time necessary for the driving procedure were measured. After the driving process, the footing was loaded with a constant rate displacement of 1 mm/min to generate an axial concentric load on the footing. A calibrated proving ring with a maximum capacity of 4.5 kN and an accuracy of 0.02 kN was used to measure the load. A 25-mm LVDT with 0.001-mm precision was used to determine the relevant footing displacement.

4.3 Scale Effect

The scale effect consisted of both the pressure level effect and the particle size effect [11]. To eliminate the particle size effect, [12] recommended model testing with B/D_{50} > (50–100). In this study, a B/D_{50} value of 206.9 was used. However, the behavior of most model-scale footing tests could not be directly related to the behavior of full-scale testing because of variations in the mean stresses encountered beneath the footings of various sizes [10]. Also, the bearing capacity in the model test would meet the theoretical prediction if the footing size was close to the real footing size [13]. To avoid such problems, reference tests were made for surface footings to explore the effect of using skirts in terms of the bearing capacity improvement ratio (BCIR).

5. TEST RESULTS

5.1 Results of Load-Settlement Curves

There are four methods for determining the ultimate stress and the corresponding ultimate settlement [14]. When no well-defined peak appears, the constant settlement to width ratio method is widely used [13]. DeBeer [15] stated that the ultimate settlement ratio ranges from 5% to 12% for the surface footing and 25% to 28% for the footing having a large foundation depth. Therefore, the ultimate bearing capacity was measured at a constant settlement ratio of 6% and 19% if no well-defined peak appeared for surface and skirted footing respectively, which agrees with the results of the verified 3D finite element models.

Two tests were performed on the surface footing as reference cases to explore the effect of using vertical skirts. Fig. 4 shows the stress-settlement curves plotted for these tests.

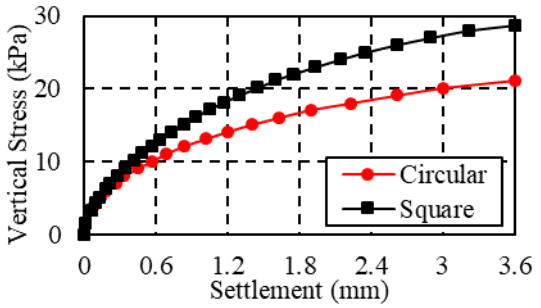

Fig. 4 Stress–settlement curves for surface footings with a width of 60 mm

The curve in Fig. 4 shows that the ultimate bearing capacity for the square footing was greater than the capacity for the circular footing by a ratio of 1.36. The reason for this behavior was the shape factor effect [16]. In this study, the theoretical bearing capacity equation for the surface footing rested over the sand is written as follows:

$$q_u = 0.5B\gamma N_\gamma \lambda_\gamma \text{ , (1)}$$

where

q_u ultimate bearing capacity;
γ soil unit weight;
B foundation width;
N_γ bearing capacity factors;
λ_γ shape factor.

The shape factor (λ_γ) is 0.6 and 0.8 for the circular and square footings, respectively. Hence, the only variable s λ_γ for both the circular and square footings with the same test condition and the same width.

The failure mechanism may be classified into three categories: general, local, and punching shear failure. Also, it was reported that the nature of the failure in the soil for the ultimate load depends on the compressibility of the soil and the ratio between the depth of the foundation and the foundation width [17]. The failure mechanism was the punching shear, as shown in Fig. 5, which agrees with the findings of [17]. Also, there was no bulging around the footing; therefore, the model dimension did not affect the results. The test findings revealed that a good degree of repeatability was obtained in the testing, which increased confidence in the sand sample preparation and equipment performance. Consequently, it was possible to infer that the experimental data supported the theoretical prediction and could be used to estimate the advantages of using a structural skirt.

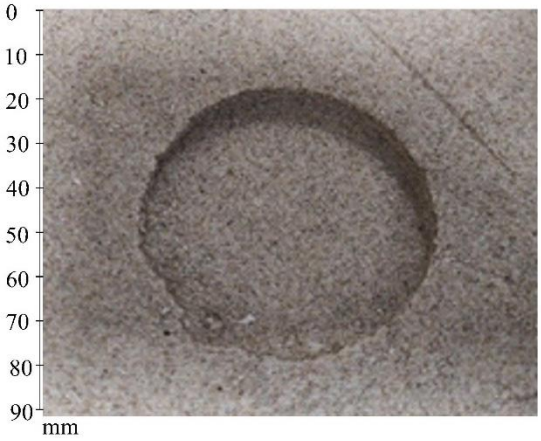

Fig. 5 Failure shape of the footing with a 60-mm diameter

Twelve tests were performed for the square and circular skirted footings. The program used is shown in Table 2. The load-settlement relationships for the circular and square footings are shown in Figs. 6 and 7, respectively.

Vesic's [17] failure mechanism may not be applicable for skirted foundations. The skirts are connected to the surface footing; therefore, they are extended to a certain depth (Ds), and they confine the soil within the skirt cell. Consequently, the footing and the skirt cell with the soil inside the function as a single system. However, the failure mechanism of a skirted foundation undergoes surface, plugged deep, and coring deep failure modes [18]

The ultimate bearing capacity for the skirted foundation was measured and compared with the reference case; the BCIR is the ratio of skirted footing ultimate load to the surface footing ultimate load and is summarized in Table 2.

Table 2 Testing programs and their results

Shape of Footing	D (mm) Or B (mm)	Relative density, D_r (%)	D_s/D Or Ds/B	BCIR
Circular	60	35	0.00	1.00
			0.25	2.55
			0.50	3.79
			0.75	5.01
			1.00	6.47
			1.25	7.85
			1.50	8.97
Square	60	35	0.00	1.00
			0.25	2.09
			0.50	2.59
			0.75	3.84
			1.00	4.20
			1.25	4.79
			1.50	5.67

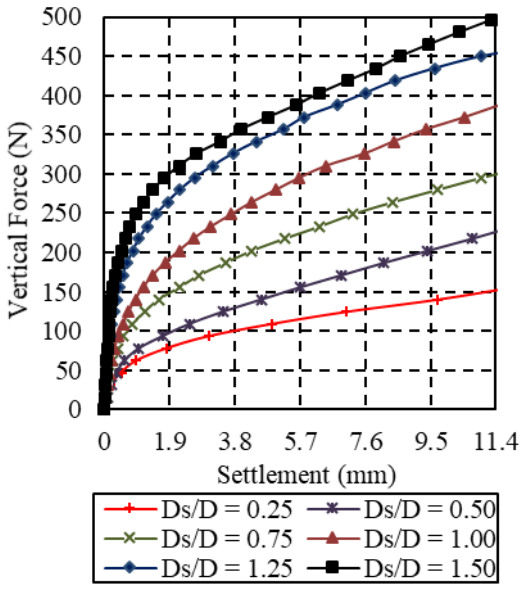

Fig. 6 Vertical force versus settlement for a circular footing having a 60-mm diameter

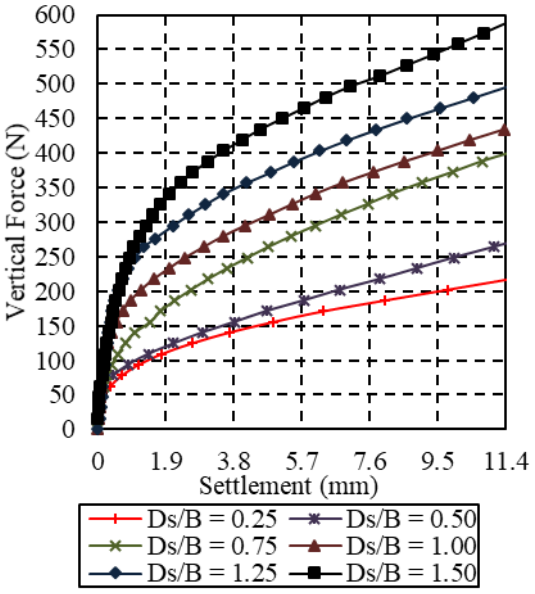

Fig. 7 Vertical force versus settlement for a 60-mm wide square footing

The results show that using skirts improves the load-settlement curves (Figs. 6 & 7). Because the depth of the foundation increases with the increase in the skirt depth. Therefore, the first term in Terzagi's equation increases. The bearing capacity equation for the shallow footing rested on a homogenous layer of sand [16] as follows:

$$q_u = \gamma D_f N_q + 0.5\, B\gamma N_\gamma \text{ , (2)}$$

Here, D_f is the depth of the lower edge of the skirt below the ground level [5] and are the bearing capacity factors.

The rise in the skirted footing bearing capacity is split into two stages. The first stage occurs when the settlement for the footing width ratio is less than 2%, and the bearing capacity reaches approximately 50% of its maximum value. The second stage reveals that when the soil settlement for the footing width ratio exceeds 2%, the load grows slowly and nearly linearly with almost no peak (Figs. 6 & 7).

5.2 The Effect of Skirt Depth

The effects of the skirt depth ratio were investigated through the value of BCIR. For the sand having a relative density of 35%, BCIR values for the square footing reached 2.09 and 5.67 for Ds/B values of 0.25 and 1.50, respectively. Also, BCIR values for the circular footing of 2.55 and 8.97 were reached for Ds/D values equal to 0.25 and 1.50, respectively (Fig. 8). The results also proved that BCIR increases as the skirt depth ratio increases.

The results of the BCIR were compared to the finding of [4,6,8]. The results of this study for square footing showed a similar trend reported in [6]. Furthermore, this comparison spells out the skirt cell size and footing size effect as the BCIR for this study for circular footing is greater than the finding of [4]. Where the confinement becomes significant for small size footings, according to [19]. Moreover, it illuminates the effectiveness of the skirted footing system in improving loose soil behavior rather than compacted soil as the results of BCIR of this study for square footing is greater than the finding of [8] (see Fig. 8).

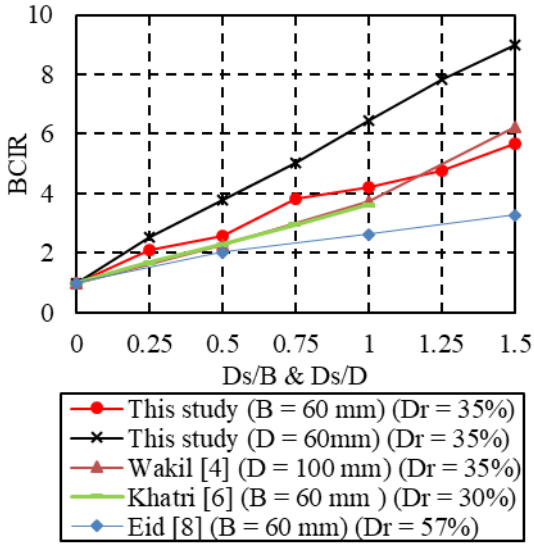

Fig. 8 Bearing capacity improvement ratio for different skirt depth ratios (D_s/D) & (D_s/B)

The relationship between the settlement

reduction factor (SRF) and skirt depth ratio (D_s/B or D_s/D) is shown in Fig. 9. The curve shows that using skirts has a great effect on settlement reduction. SRF is the ratio between the settlement of the skirted foundation (S_s) at the surface ultimate load to the settlement of the surface footing (S_u) at the same load.

It was observed that the SRF decreased steadily as the skirt depth increased. For the square skirted footing, the settlement reduction (the decrease in the surface ultimate settlement) was 61.79% and 95.10% for skirt depth ratios of 0.25 and 1.50, respectively. For the circular skirted footing, the settlement reduction was 84.11% and 98.65% for skirt depth ratios of 0.25 and 1.50, respectively.

The SRF is compared with the finding of [7,8] in Fig. 9. The results reveal that this study follows a similar trend reported in [7,8]. This comparison illuminates the effectiveness of using skirted foundation in loose sand rather than compacted sand and for small-footing size as a settlement reducer. Where the reduction in settlement for the current study is greater than the finding of [7,8] (see Fig. 9).

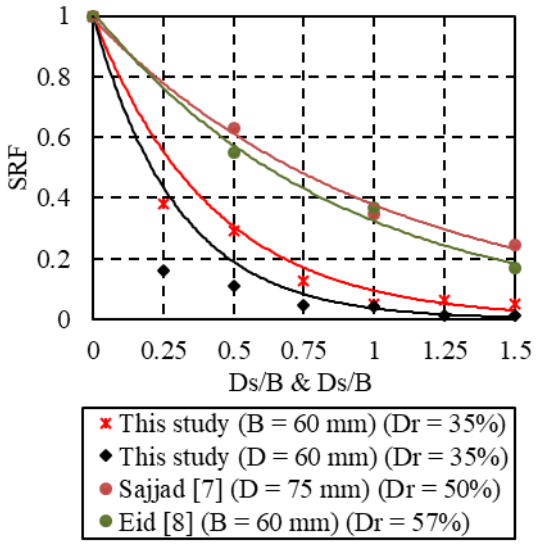

Fig. 9 Settlement reduction factor versus skirt depth ratio

5.3 Skirt Cell Shape and Footing Shape Effect

The skirt cell shape affects the behavior of the skirted foundation. It can be shown that for the surface footing, the shape effect appears where the bearing capacity of the square footing is 1.36 times higher than that of the circular footing. However, for the skirted footing with a skirt depth ratio of 0.25 to 0.75, the skirt cell shape effect covers the previous effect of the shape factor; therefore, the bearing capacity reaches equilibrium for both the square and circular footings (Fig. 10). When the skirt depth ratio is greater than 0.75, the skirt cell shape factor becomes dominant. Where the bearing capacity of the square skirted footing starts to decrease. Therefore, the improvement was found to be greater for circular footing than square and increased with the increase in skirt depth. The ratio between the ultimate bearing capacity of the square footing to circular is 1.36, 1.04, and 0.86 for skirt depth ratios of 0, 0.75, and 1.50 (see Fig. 10).

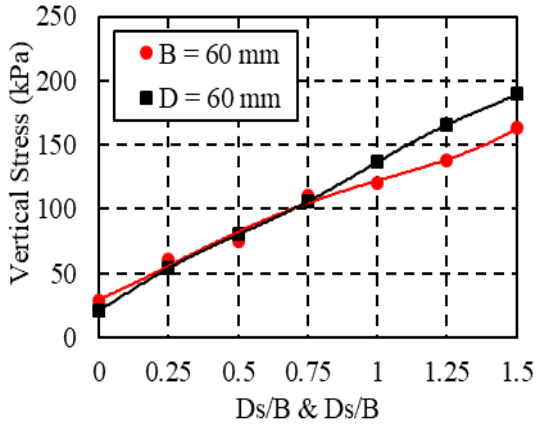

Fig. 10 Vertical stress versus skirt depth ratios for the two footing shapes

6. NUMERICAL ANALYSIS

The Plaxis 3D foundation software package was used to perform 3D finite element analysis [20]. The experimental results were simulated to verify the 3D finite element model.

The sand was represented using 10-node triangular elements, whereas the footing and skirting were composed of a 6-node triangular plate element and a 12-node triangle for the interface element. The geometry of the model was taken as the current setup of the experiment (see Fig. 11). The soil properties are listed in Table 3; these values were obtained from laboratory tests. Other undefined parameters were derived using multiple attempts and literature correlations to match the experimental results. Table 4 lists the footing and skirt properties.

The model mesh size was medium, and a local mesh with a finer mesh size was defined around the footing zone to reduce the time analysis process.

The calculation process was performed in three phases starting from an initial phase where the Ko procedure was used to develop initial stresses. The footings, skirts, and interfaces were activated in phase two, and plastic analysis was assigned. Through the final phase, the prescribed displacement was activated, and plastic analysis was assigned.

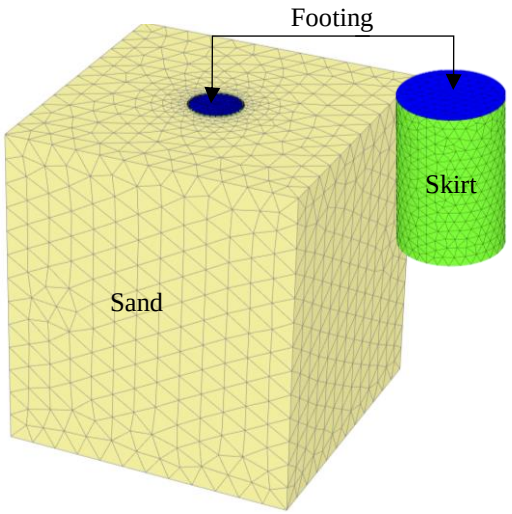

Fig. 11 Circular footing model geometry and mesh generation for (D_s/D =1.00)

Table 3 Soil parameters of the sand used for the verification analysis

Soil Parameter	Sand
Constitutive model	Hardening
Drainage type	Drained
Unit weight (kN/m^3)	15.59
Reloading/preloading Poisson's ratio (υ_{ur})	0.20
Peak friction angle (ϕ^o)	34.50
The angle of dilatancy (ψ^o)	4.50
Interface strength factor (R_{in})	0.70
Power (m)	0.50
Void ratio (e)	0.7188

The secant stiffness E_{50}^{ref} (kN/m^2) was assumed to be R_D*60 (Mpa) [21]; the tangent stiffness was assumed to be equal to the secant stiffness E_{50}^{ref} (kN/m^2), and the unloading/reloading stiffness was assumed to be equal to three times the secant stiffness E_{50}^{ref} (kN/m^2) [22].

Table 4 Footing and skirts parameters used in verification analysis

Soil Parameter	Footing	Skirts
Material	Steel	
Constitutive Model	Linear elastic	
Unit weight (kN/m^3)	78	
Poisson's ratio	0.2	
Young's modulus (kN/m^2)	20×10^7	

6.1 Model Verifications

For the skirted footing, the 3D finite element curve shows a slightly different trend than the experimental results (Fig. 12). This could be attributed to the skirted footing's installation effect. In experimental studies, installing the skirts into the sand produces a slight change in the relative density. Therefore, the experimental curve follows a stiffer response at first followed by a progressive increase in the load. This difference in results follows the same pattern as [9].

For the same ultimate settlement, the ultimate load obtained from the 3D finite element models coincided with the ultimate load developed from the experimental investigations (Fig. 13). The overall difference between the results of the finite element models and this research was minimal.

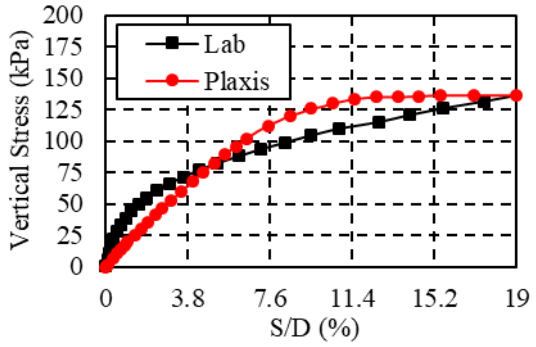

Fig. 12 Vertical stress versus settlement ratio for circular footing with a skirt depth ratio of 1.00

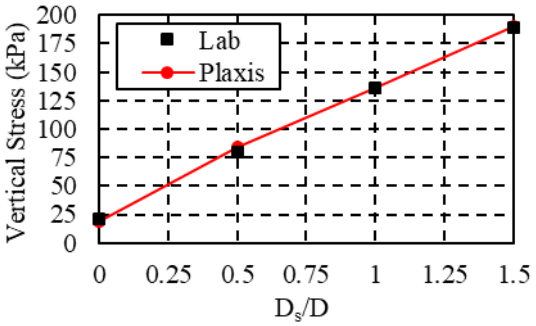

Fig. 13 Vertical stress versus skirt depth ratio for circular footing

7. CONCLUSION

From the developed experimental tests and numerical models, the following may be concluded:

Using skirts beneath the footing improved the overall behavior of load-settlement curves because they increased the bearing capacity; this was illustrated by the BCIR values. The skirted footing also reduced the settlement that was defined through the SRF. The increase in the bearing capacity increases with the increase in the skirt depth ratio. However, the increase in skirt depth

ratio decreases the settlement

The increase in the bearing capacity of the skirted footing reached ~50% of its ultimate value at the low settlement ratio (S/B or S/D) of 2%. Therefore, the skirted footing is an effective settlement reducer system.

The improvement in the load-settlement behavior of shallow footing is greater for footing resting over loose sand than that over compacted sand and for smaller footing size.

The skirt cell shape effect increases with the increase in skirt depth. This effect improves the load-settlement behavior to be greater for the circular shape than the square when both had the same width and skirt depth.

The comparison between the 3D finite element results and the experimental small-scale models showed acceptable agreement.

8. REFERENCES

[1] Bransby F. and Randolph M., Combined Loading of Skirted Foundations, Geotechnique, Vol. 48, 1998, pp. 637-655.

[2] Dewoolkar M., Hwang J., and Ko H.Y., Physical and Finite Element Modeling of Lateral Stability of Offshore Skirted Gravity Structures Subjected to Iceberg Impact Load, Ocean Engineering, Vol. 35, 2008, pp. 1615-1626.

[3] Byrne B. and Houlsby G., Experimental Investigations of Response of Suction Caissons to Transient Vertical Loading, Journal of Geotechnical and Geoenvironmental Engineering, Vol. 128, 2002.

[4] Wakil A., Bearing Capacity of Skirt Circular Footing on Sand, Alexandria Engineering Journal, Vol. 52, 2013, pp. 359-364.

[5] Al Aghbari M. and Mohamedzein Y., Bearing Capacity of Strip Foundations with Structural Skirts, Geotechnical, and Geological Engineering, Vol. 22, 2004, pp. 43-57.

[6] Khatri V., Debbarma S.P., Dutta R.K., and Mohanty B., Pressure-Settlement Behavior of Square and Rectangular Skirted Footings Resting on Sand, Geomechanics and Engineering, Vol. 12, 2017, pp. 689-705.

[7] Sajjad G., and Makarchian M,, Study of the behavior of skirted shallow foundations resting on the and, International Journal of Physical Modelling in Geotechnics, vol. 18, 2018, pp. 117-130.

[8] Eid H., Bearing Capacity and Settlement of Skirted Shallow Foundations on Sand, International Journal of Geomechanics, Vol. 13, 2013, pp. 645-652.

[9] Zeydi H. and Boushehrian A., Experimental and Numerical Study of Bearing Capacity of Circular Footings on Layered Soils With and Without Skirted Sand Piles, Iranian Journal of Science and Technology, Transactions of Civil Engineering, Vol. 44, 2019.

[10] Cerato A. and Lutenegger A.J., Scale Effects of Shallow Foundation Bearing Capacity on Granular Material, Journal of Geotechnical and Geoenvironmental Engineering, Vol. 133, 2007, pp. 1192-1202.

[11] Siddiquee M., Tanaka T., Tatsuoka F., Tani K., and Morimoto T., Numerical Simulation of Bearing Capacity Characteristics of Strip Footing on Sand, Soils, and Foundations, Vol. 39, 1999, pp. 93-109.

[12] Kusakabe O., Foundations, in R.N. Taylor (Ed.), Geotech. Centrifuge Technology, Vol. 37, Blackie Academi & Professional, London, 1995, pp. 828-842, Cand. Geotechnical J. (Chapter 6).

[13] As'ad M., Bearing Capacity Improvement of Shallow Foundation on Multilayered Geogrid Reinforced Sand, Geomate Journal, Vol. 18, Issue 69, 2020, pp. 216-223.

[14] Lutenegger A.J., and Adams M.T., Bearing Capacity of Footings on Compacted Sand, 1998.

[15] DeBeer E.E., Proefondervindelijke bijdrage tot de studie van het gransdraagvermogen van zand onder funderingen op staal, Bepaling von der vormfactor sb, Annales des Travaux Publics de Belgique, 1967.

[16] Terzaghi K., Theoretical Soil Mechanics, New York: Wiley, 1943.

[17] Vesic A.S., Bearing Capacity of Shallow Foundations, Foundation Engineering Handbook, Winterkorn and Fang, 1975.

[18] Schneider J., and Senders M., Foundation Design: A Comparison of Oil and Gas Platforms with Offshore Wind Turbines, Marine Technology Society Journal, vol. 44, 2010, pp. 32-51.

[19] Prasad A.M., Silva L.I.N.D., and Chaminda G., The Effect of Lateral Confinement on the Settlement Characteristics of Shallow Foundations on Sand, Geomate Journal, Vol. 15, Issue 51, 2018, pp. 258-265.

[20] Brinkgreve R. and Broere W., Plaxis 3D Foundation Version 1, 2004.

[21] Lengkeek H.J., Estimation of Sand Stiffness Parameters from Cone Resistance, 2003.

[22] Schanz T., Vermeer P.A., and Bonnier P.G., The Hardening Soil Model: Formulation and Verification, 2019, pp. 281-296.